



Contents lists available at ScienceDirect

Journal of Plant Physiology

journal homepage: www.elsevier.com/locate/jplph

Physiology

Light-harvesting complex B7 shifts the irradiance response of photosynthetic light-harvesting regulation in leaves of *Arabidopsis thaliana*

Richard B. Peterson*, Neil P. Schultes

Department of Biochemistry and Genetics, The Connecticut Agricultural Experiment Station, 123 Huntington Street, New Haven, CT 06511, USA

ARTICLE INFO

Article history:

Received 10 June 2013

Received in revised form

10 September 2013

Accepted 10 September 2013

Available online xxx

Keywords:

810-nm transmittance

Chlorophyll fluorescence

LHC7

Non-photochemical quenching

Photosystem

Quantum yield

ABSTRACT

The nuclear LHC7 gene is common in higher plants, encodes a transcript that is well expressed in a subset of leaf mesophyll cells, and is associated with a protein product that is homologous to pigment-binding components of the photosystem (PS) II peripheral antenna complex. We compared the physiological properties of wild type and LHC7-deficient leaves [DNA insertion, *Arabidopsis thaliana* (At) ecotype Columbia] in terms of pigment content, CO₂ exchange, *in vivo* transmittance at 810 nm, and chlorophyll fluorescence. The latter two techniques are functional indicators for PSII and PSII, respectively. Key features of the mutant phenotype were confirmed using antisense technology and a hemizygote of two independent AtLHC7 DNA insertion lines. Growth, leaf pigment composition, white light absorptance, and levels of AtLHC7-6 were not significantly different in the mutant compared to wild type. Likewise, neither intrinsic PSII light capture efficiency nor partitioning of absorbed radiation to PSII was affected by the mutation. The absence of AtLHC7 is associated with lower rates of light-saturated photosynthesis and a diminished irradiance threshold for induction of photoprotective non-photochemical quenching. Overall, the pattern of change in light utilization parameters and plastoquinol level indicated that loss of AtLHC7 expression led to slower Rubisco turnover characterized by pH-dependent balancing of electron transport to reduced carbon assimilation capacity (photosynthetic control). No effect of AtLHC7 genotype on xanthophyll de-epoxidation state was detected suggesting that factors in addition to luminal pH influence zeaxanthin accumulation.

© 2013 Elsevier GmbH. All rights reserved.

Introduction

Chloroplastic pigment-binding proteins of higher plant light-harvesting complexes (LHCs) capture radiant energy that drives the primary redox reactions of photosynthesis. The LHCA and LHC families comprise the peripheral antennae of Photosystems I and II (PSI and PSII), respectively (Green and Durnford, 1996). In the

higher plant model *Arabidopsis thaliana* (At), approximately 30 nuclear LHC superfamily loci encode the LHCA and LHC proteins, early light-inducible proteins (ELIPs), ferrochelatase and psbS (Jansson, 1999). Currently, nine LHC families have been identified based on comparisons of amino acid sequence similarity across species (i.e. LHC1-9). In *Arabidopsis* and other higher plants, the major LHC proteins LHC1, LHC2, and LHC4 are encoded by multigene families while LHC3, LHC5, LHC6 are encoded by single loci. The outermost PSII antenna proteins (LHC1-3) normally exist as heterotrimers. The LHC4-6 monomers connect the trimer complexes to the PSII core containing the photochemical reaction center (Dekker and Boekema, 2005; Allen et al., 2011).

Two novel *Arabidopsis* chlorophyll (Chl) *a/b*-binding proteins, AtLHC7 and AtLHC8 (previously AtLHC4.3) were inferred from a subset of "rarely expressed" LHC genes based on expression patterns across different tissues or laboratory conditions (Klimmek et al., 2006). Later, a new locus apparently unique to *Physcomitrella patens* was designated as LHC9 (Alboresi et al., 2008). Overall expression patterns were similar for AtLHC7 and AtLHC8 but differed substantially from the 10 abundant LHCs (AtLHC1-4 and AtLHC1-6). Association of these proteins with the peripheral

Abbreviations: A, antheraxanthin; ANOVA, analysis of variance; CA, complementary area; Chl, chlorophyll; Col, ecotype Columbia; Cyt, cytochrome; F_o, F_s, F_m, fluorescence yields: minimum, steady-state, maximum; FR, far red light; HL, high light; LE, ecotype Landsberg erecta; LHC, light-harvesting complex; LL, low light; LHCA, LHC, light-harvesting complexes of photosystem I, II; ML, medium light; NPQ, non-photochemical quenching; p, probability; PAD, photon absorption density ($\mu\text{mol m}^{-2} \text{s}^{-1}$); PFD, incident photon density ($\mu\text{mol m}^{-2} \text{s}^{-1}$); PC, plastocyanin; PQ(H₂), plastoquinone (reduced); PSI, PSII, photosystem I, II; P680, primary electron donor of PSII; Q_A, Q_B, photosystem II acceptor side quinone electron carriers; R², coefficient of determination; (RT)-PCR, (reverse transcriptase)-polymerase chain reaction; SE, standard error of the mean; V, violaxanthin; WL, white light; WT, wild type; Z, zeaxanthin.

* Corresponding author. Tel.: +1 203 974 8463; fax: +1 203 974 8502.

E-mail address: Richard.Peterson@ct.gov (R.B. Peterson).

light-harvesting complex of PSII was inferred by sequence homology (LHC B7 is closest to LHC B5) and low interspecies similarities (Klimmek et al., 2006). Characteristic LHC B structural features such as pigment-binding sites, transmembrane helices, and a trimerization motif were conserved for AtLHC B7. It occurs widely in land plants but not algae consistent with a role in adaptation to a dynamic light environment (Klimmek et al., 2006; Alboresi et al., 2008).

Information on individual function among the structurally redundant LHC B proteins has been sought using T-DNA and antisense technology. LHC-deficient plants invariably retained the ability to grow autotrophically. Nevertheless, co-suppression of AtLHC B1/AtLHC B2 and of loss of AtLHC B6 modestly reduced the capacity to form the pH-dependent, rapidly reversible phase (qE) of non-photochemical quenching (NPQ) (Andersson et al., 2003; Kovács et al., 2006; Bianchi et al., 2008). Although CO₂ uptake rates were unaffected by loss of AtLHC B1/AtLHC B2 a significant decline in PSII photochemical efficiency [$(F_m - F_o)/F_m$] for dark-adapted leaves indicated some destabilization of PSII macro-organization (Andersson et al., 2003). Antisense inhibition of AtLHC B5 and AtLHC B4 accumulation had no effect on qE and about 25% loss of qE , respectively (Andersson et al., 2001). On the other hand, photosynthetic rates were slightly lower for the AtLHC B4-deficient line but were enhanced by suppression of AtLHC B5 accumulation. Dark-adapted F_v/F_m values indicated some changes in organization of the light-harvesting antennae (Andersson et al., 2001). In contrast to the mild effects of LHC loss on growth under controlled conditions, prolonged exposure of these *Arabidopsis* lines to natural conditions often resulted in reduced fitness (Andersson et al., 2003; Ganeteg et al., 2004). Thus, slight structural variations cumulatively confer functional flexibility needed for robust growth in fluctuating light.

The role of AtLHC B7 in photosynthetic light-harvesting has not heretofore been explored. Insertional mutagenesis often results in complete loss of gene function (O'Malley and Ecker, 2010). Alternative approaches based on antisense, RNAi, or chemically-induced point mutations can result in some accumulation of a functional product. We describe compositional and functional consequences of DNA insertion into the sole AtLHC B7 locus (At1g76570).

Materials and methods

Plant material and growth conditions

Seed of *Arabidopsis thaliana* (L.) Heynh. lines SALK_018360C [ecotype Columbia (Col); Alonso et al., 2003] and WiscDsLox 506A05 (Col; Woody et al., 2007) were obtained from The *Arabidopsis* Biological Resource Center. A third line, GT20564 [ecotype Landsberg erecta (LE); Sundaresan et al., 1995], was obtained from Cold Spring Harbor Laboratory. Each line reportedly contained a unique DNA insertion into AtLHC B7 (At1g76570). Plants were grown in a growth chamber in fertilized Super Fine Germinating Mix (Conrad Fafard, Agawam, MA) at an incident photon flux density (PFD) of 130 μmol quanta m⁻² s⁻¹ and a 16/8 h day/night regime and 23/20 °C. Light was supplied by a combination of Cool White fluorescent and incandescent lamps. Fully expanded rosette leaves were examined at 3–4 weeks after sowing.

Gas exchange and optical methods

The two-channel fast-response leaf gas exchange measurement system (Fast-Est, Tartu, Estonia) has been described (Laisk et al., 2002; Peterson, 2005). An excised leaf was enclosed in a temperature-controlled (leaf temperature of 22.8–23.2 °C), flow-through sandwich-type chamber and flushed with gas (380 μmol CO₂ mol⁻¹, 2.0% O₂, balance N₂) at 0.5 mmol s⁻¹. Distilled H₂O was provided to the petiole. Uptake of CO₂ was

monitored with an infrared gas analyzer LI 6252 (Licor, Lincoln, NE, USA) and a micro-psychrometer detected transpiration. Calculation of dissolved CO₂ concentration at the carboxylation site (C_c, μM) considered stomatal and liquid phase diffusion resistances. The linear electron transport rate (J_c, see Laisk and Loreto, 1996) associated with photosynthetic carbon metabolism was calculated as:

$$J_c = 4(A + R_k) \frac{2K_s C_c + 2O_c}{2K_s C_c - O_c} \quad (1)$$

where A is the rate of net CO₂ assimilation (μmol m⁻² s⁻¹), R_k is Krebs cycle respiration in the light, K_s is the Rubisco CO₂/O₂ specificity factor (105 at 23 °C; Peterson and Havir, 2001), and C_c and O_c are the carboxylation site dissolved CO₂ and O₂ concentrations (μM). At limiting irradiance R_k was assumed to equal the rate of CO₂ evolution measured in prior darkness. At higher irradiances the R_k observed previously in *Arabidopsis* (0.106 μmol CO₂ m⁻² s⁻¹) was employed (Peterson and Havir, 2001). All light beams were directed to the adaxial leaf surface by a multi-branched fiber optic guide (Fast-Est, Tartu, Estonia). Actinic white light (WL) and fluorescence saturation pulses (10000 μmol quanta m⁻² s⁻¹ for 1.5 s) were provided by Schott KL 1500 tungsten halogen sources. A calibrated Licor Quantum Sensor (400–700 nm) mounted in the illumination apparatus continuously monitored the actinic PFD at the leaf surface. Far red light (FR, 50 μmol quanta m⁻² s⁻¹, 720 nm) was provided by a feedback-stabilized light-emitting diode source (Fast-Est, Tartu, Estonia). Sequence and execution of measuring procedures were standardized by use of a command textfile in conjunction with the control/acquisition software.

Chl fluorescence yield was measured with a PAM-101 equipped with an ED101 emitter-detector unit (H. Walz, Effeltrich, Germany). The quantum yield of PSII electron transport (ϕ_2) is based on the model of Genty et al. (1989):

$$\phi_2 = \frac{F_v}{F_m} \times qP = \frac{F_m - F_s}{F_m} \quad (2)$$

where

$$qP = \frac{F_m - F_s}{F_m - F_o} \quad (3)$$

Note that fluorescence yields F_m and F_o correspond to qP=0 and qP=1, respectively, and F_v=F_m–F_o. The coefficient for partitioning of absorbed WL quanta to PSII (a_2) was measured at limiting irradiance as described by Peterson et al. (2001):

$$a_2 = \frac{J_c}{PAD \times \phi_2} \quad (4)$$

NPQ is expressed as the rate constant for H⁺-regulated de-excitation in PSII (Laisk et al., 2002):

$$NPQ = \frac{F_{md}}{F_m} - 1 \quad (5)$$

F_{md} is the “predawn” maximum yield measured after ≥12 h of darkness. Other details pertaining to signal processing have been described (Peterson et al., 2001; Peterson, 2005).

Changes in leaf transmittance at 810 nm were employed as a probe of PSI function using a single beam spectrophotometer FS810A (Fast-Est, Tartu, Estonia; Talts et al., 2007). The modulated (80 kHz) measuring beam was directed to a 1-cm² area at the center of the adaxial side of the test leaf. A photodetector facing the abaxial side registered transmission. Increased absorption of 810-nm radiation due to accumulation of P700⁺, oxidized plastocyanin (PC⁺), and reduced ferredoxin was isolated after compensation of the full signal voltage, amplified prior to processing by a 12-bit analog-to-digital converter, and displayed as a positive change. Electro-pneumatic shutters (flying time of 1.3 ms) enabled recording of rapid, irradiance-dependent changes in the 810-nm signal.

A shortpass filter in the ED101 detector channel facilitated simultaneous recording of fluorescence and 810-nm transmission signals.

Each test leaf (pre-darkened ≥ 12 h) was mounted in the chamber, followed by recording of predawn fluorescence yields (F_{od} and F_{md} ; Peterson et al., 2001). The leaf was then pre-illuminated at a PFD of $200 \mu\text{mol quanta m}^{-2} \text{s}^{-1}$ until steady state photosynthesis was attained. The stable CO_2 uptake rate; light-adapted fluorescence yields F_s , F_m , and F_o ; and light-dark 810-nm transmittance changes (six-fold signal averaging) were recorded for successive WL test irradiances (Peterson, 2005). Measurement of F_o included a 3-s exposure to FR to fully oxidize the PSII acceptor side as described by Peterson and Havar (2004). Total (400–700 nm) leaf absorptance for actinic WL (α) was measured with an integrating sphere using a KL 1500 tungsten halogen source (Peterson and Havar, 2001). The photon absorption density (PAD) was calculated from the incident photon flux density (PFD) as $\text{PAD} = \alpha \times \text{PFD}$.

Pigment analyses and immunoblots

Pigment separation by HPLC of 80% acetone extracts of leaf tissue has been described (Peterson and Havar, 2000). Immunoblots of psbS (Peterson and Havar, 2004) and LHCb proteins in leaf membranes were performed according to manufacturer (Agrisera) recommendations.

DNA and RNA manipulations

DNA was extracted from leaves according to Dellaporta (1993). RNA isolation was carried out using TRIzol (Invitrogen, Carlsbad, CA) and reverse transcription of RNA with a RCM-RACE Kit (Ambion, Austin, TX) according to manufacturer recommendations. Oligonucleotide primers AtLHC7A (5'ATGGCACTGTTTCAAGGAGAAC 3'), AtLHC7C (5'GAAACCATAATCCCTGAAG 3'), and P745 (5'AACGTCCGCAATGTGTTATTAAAGTTGTC3') were used to genotype individual plants in a segregating population of WiscDsLox506A05 by PCR. Oligonucleotides AtLHC7A, AtLHC7E (5'AACTGCAGTCATGTCTGAAGCATGGCAATCAG 3') and Lb (5'CATTITATAATAACGCTGCCGACATCTAC 3') were used to genotype plants in the CSHL GT20564 lines. Primers AtLHC7A and AtLHC7C were used to amplify a 408-bp AtLHC7-derived cDNA fragment from reverse transcribed Col leaf RNA and cloned into pCR2.1-TOPO (Invitrogen, Grand Island, NY) to form plasmid pRH527. pRH527 was restricted with endonucleases KpnI and PstI to clone the AtLHC7 fragment in antisense orientation in binary plasmid pRH118 [composed of pCAMBIA1200 (Genbank# AF234292) and the 35S cassette from pFF19 (Timmermans et al., 1990)] to form plasmid pRH529. pRH529 was transformed into *Agrobacterium tumefaciens* GV2260 and used to transform Col by the floral dip method (Clough and Bent, 1998). Oligonucleotides AtLHC7A and AtLHC7C were used in reverse transcriptase-PCR (RT-PCR) analyses. The PCR parameters employed were: 94 °C 3 min; [94 °C 30 s, 55 °C 30 s, 72 °C 1 min] repeated 30× followed by 72 °C 7 min.

Results

Molecular characterization of AtLHC7-deficient lines

Locus At1g76570 contains six exons (Fig. 1A) encoding a unique protein designated as AtLHC7 by Klimmek et al. (2006). Three lines were reported to contain DNA insertions in exons of At1g76570. Lines WiscDsLox506A05 and GT20564 harbor T-DNA and “gene trap” insertions, respectively. Fig. 1B shows PCR results for homozygous wild type (WT) and mutant plants from a segregating population of WiscDsLox506A05. This mutant allele is designated *Atlhcb7-1*. Line GT20564, as obtained, was homozygous for the insertion in exon 3 (Fig. 1C) and designated *Atlhcb7-2*.

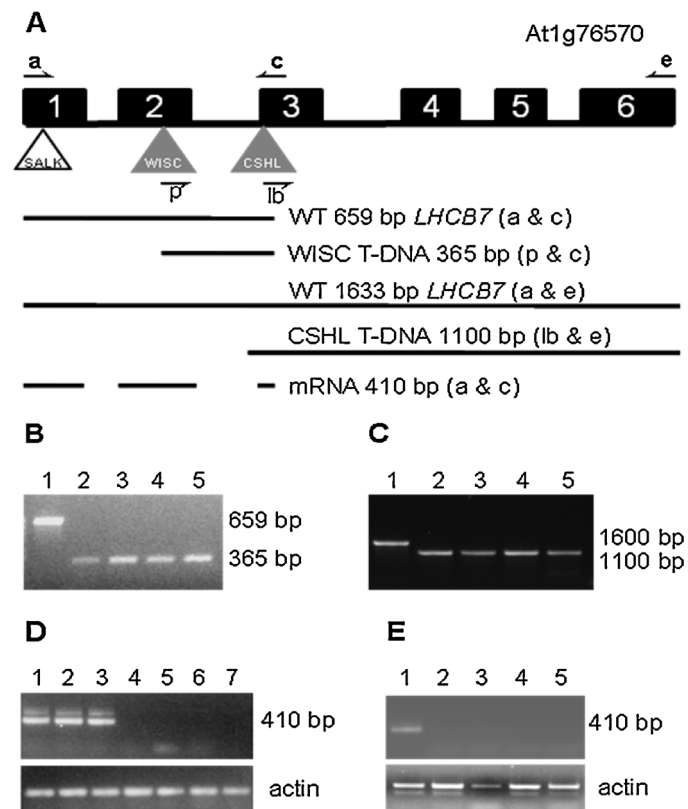


Fig. 1. Molecular analysis of the At1g76570 gene. (A) At1g76570 structure. Boxes and lines represent exon and intron sequences, respectively. Triangles correspond to putative T-DNA insertions. Gray triangles labeled WISC (line WiscDsLox506A05, insertion in exon 2) and CSHL (GT20564, insertion in exon 3) correspond to loci confirmed below. A reported insertion at the open triangle labeled SALK (SALK_018360C) in exon 1 was not confirmed (see text). Arrows a, c, e, p and lb denote the positions and orientations of oligonucleotide primers AtLHC7A, AtLHC7C, AtLHC7E, P745 and lb, respectively (see Materials and methods). The DNA fragment sizes (base pairs, bp) generated by PCR for WT and insertion mutant chromosomes are indicated. A 410-bp DNA fragment is generated upon RT-PCR treatment of At1g76570-specific mRNA transcripts (primers a and c). (B) Genotype analysis for the WISC locus (*Atlhcb7-1*). Lane 1 shows the 659-bp DNA band resulting from PCR treatment of genomic DNA from WT segregants while lanes 2–5 contain a 365-bp fragment derived from homozygous mutant tissues. (C) Genotype analysis for the CSHL locus (*Atlhcb7-2*). Lane 1 shows the 1600-bp DNA band resulting from PCR treatment of genomic DNA from WT tissue while lanes 2–5 contain a 1100-bp fragment derived from homozygous mutant tissues. (D) Expression analysis of WT Col and *Atlhcb7-1* mutant tissue. Shown are results of RT-PCR treatment of mRNA from homozygous WT leaves (lanes 1–3) and homozygous mutant leaves (lanes 4–7) for At1g76570- and actin-specific products. (E) Expression analysis of WT ecotype Landsberg erecta (LE) and *Atlhcb7-2* mutant tissue. Shown are results of RT-PCR treatment of mRNA from homozygous WT leaves (lane 1) and homozygous mutant leaves (lanes 2–5) for At1g76570- and actin-specific products.

Homozygous mutant plants are hereafter referred to by allele designations. Sequencing of DNA revealed that SALK_018360C does not contain an insertion in exon 1 (Fig. 1A) as reported by Alonso et al. (2003). Instead, a T-DNA insertion was found upstream of exon 1 in an orientation compatible with AtLHC7 expression. Analysis of At1g76570 mRNA by (reverse transcriptase)-polymerase chain reaction (RT-PCR) showed that homozygous WT leaves generated a 410-bp AtLHC7-specific DNA fragment while no AtLHC7 transcript was observed for *Atlhcb7-1* and *Atlhcb7-2* plants (Fig. 1D and E). Thus, molecular genotypes correlate with AtLHC7 transcript accumulation confirming that *Atlhcb7-1* and *Atlhcb7-2* are true knockouts (null alleles) of At1g76570. Line WiscDsLox506A05 segregated WT siblings which served as ideal controls for physiological assessments. Since an isogenic WT strain could not be confirmed for *Atlhcb7-2* we focus on the properties of *Atlhcb7-1*, an antisense strain prepared in Col, and a hemizygous knockout

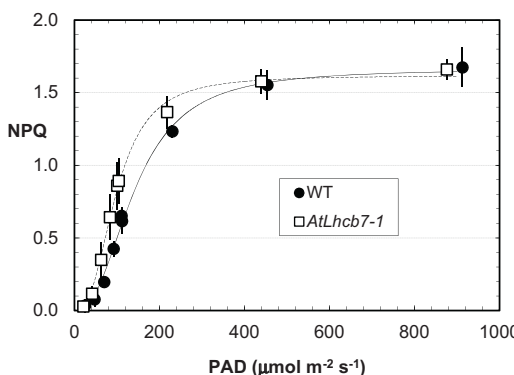


Fig. 2. Dependence of NPQ on PAD for WT (Col) and AtLhcb7-1. Each point is a mean of four measurements performed on separate leaves. The sequence of nominal PFD levels for each light curve was 120, 100, 75, 50, 25, 120, 250, 500, 1000 $\mu\text{mol quanta m}^{-2} \text{s}^{-1}$. Error bars indicate $\pm\text{SE}$. The lines are fits to the respective data sets using a sigmoid function.

obtained as an F1 cross of AtLhcb7-1 and AtLhcb7-2 (AtLhcb7-1/2).

AtLHCB7-deficiency does not alter the contents of pigments or major PSII antenna proteins

Homozygous AtLhcb7-1 plants were not discernibly affected in appearance or growth compared to WT. Leaf pigment levels [10–30 replicates (N) per line] were not significantly different at the 5% probability level based on a T-test (i.e. $p > 0.05$). The overall average [\pm standard error (SE)] Chl $a+b$ content was $195 \pm 6 \mu\text{mol m}^{-2}$ and the Chl a/b was $2.66 \pm 0.04 \text{ mol mol}^{-1}$. Combined xanthophyll cycle [violaxanthin (V)+antheraxanthin (A)+zeaxanthin (Z)], lutein, neoxanthin, and β -carotene levels were 0.186 ± 0.006 , 0.639 ± 0.010 , 0.127 ± 0.001 , and $0.305 \pm 0.004 \text{ mol (mol Chl } a)^{-1}$, respectively. Consistent with the pigment data, respective mean leaf white light (WL) absorptances for WT and AtLhcb7-1 were $0.825 \pm 0.012 (N=7)$ and $0.810 \pm 0.012 (N=10)$ and not statistically different. Immunoblots of leaf membrane proteins from WT and AtLhcb7-1 were identical with respect to AtLHC1-6 and AtPsbS contents (not shown).

Contrasting light utilization properties of WT and AtLhcb7-1

Although identical in saturating light, the rise in NPQ (Eq. (5)) in low light is shifted to a lower irradiance range for the mutant (Fig. 2). Two-way analysis of variance (ANOVA) indicated that the effect of genotype is significant ($p = 0.025$). We note that maximum fluorescence yields: (F_m) was measured after 80–120 s at each irradiance level. Repeated measurements of NPQ at a nominal incident photon density ($\mu\text{mol m}^{-2} \text{s}^{-1}$) (PFD) of $120 \mu\text{mol m}^{-2} \text{s}^{-1}$ (see legend to Fig. 2) were reproducible indicating an absence of latency for both lines. Although the familiar formula for NPQ reflects changes in F_m (PSII reaction centers closed), increased thermal dissipation also lowered emission when centers were open (minimum fluorescence yield: (F_0)). Plots of F_{md}/F_0 versus F_{md}/F_m (not shown) for WT and mutant were linear (slope = 1.37 ± 0.04) yet indistinguishable consistent with a common antenna-based quenching mechanism (Dau, 1994; see also Peterson and Havar, 2004).

The redox state of the initial quinone electron acceptor in PSII (Q_A) is given by qP (Eq. (3)). Fig. 3 shows the irradiance responses of qP , the quantum yield of linear electron transport supporting carbon metabolism ($\phi_s = J_c/PAD$, Eq. (1)), and PSII photochemical yield (ϕ_2 , Eq. (2)). Nearly identical results were obtained for WT and mutant in limiting light. However, a shift in downregulation

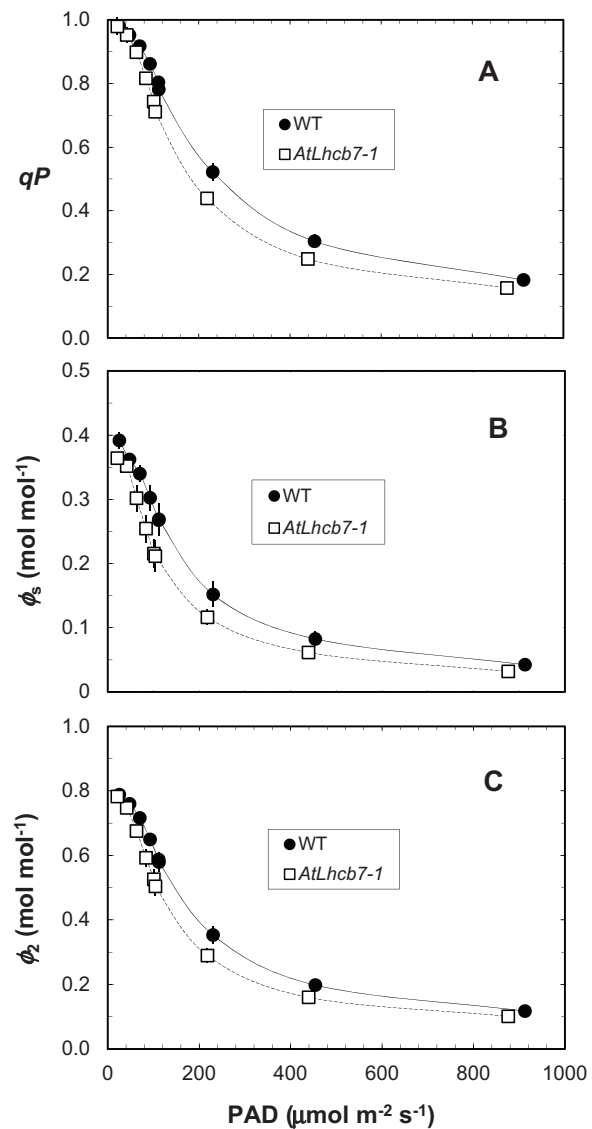


Fig. 3. Dependence of the oxidation state of Q_A , qP (panel A); quantum yield of linear electron transport supporting carbon metabolism, $\phi_s = J_c/PAD$ (panel B, see Eq. (1)); and photochemical quantum yield of PSII, ϕ_2 (panel C, see Eq. (2)) on PAD. Data obtained from the experiments of Fig. 2.

of light use efficiency to a lower irradiance range in AtLhcb7-1 occurred as light became progressively less limiting. Two-way ANOVA indicated a highly significant effect of genotype for each of these parameters ($p < 0.001$). Plots of ϕ_s (Fig. 3B) versus ϕ_2 (Fig. 3C) were quasi-linear yet undistinguishable for WT and mutant (not shown). Table 1 summarizes the properties of WT and AtLhcb7-1 using a measuring protocol targeted to limiting (low light (LL)), intermediate (medium light (ML)), and saturating (high light (HL)) light. There was no significant effect of AtLHCB7 genotype on PSII “predawn” quantum yield (F_v/F_{md}) or the fraction of absorbed WL quanta partitioned to PSII (a_2 , Eq. (4)). Although mean stomatal resistance to CO_2 diffusion (R_w) was slightly higher in AtLhcb7-1, this effect was statistically insignificant ($p > 0.05$). Conversely, effects of AtLHCB7 expression on J_c , NPQ, qP , and ϕ_2 were significant indicating higher PSII photochemical yield for WT. Higher PSII excitation capture efficiency (F_v/F_m , Eq. (2)) for WT is consistent with the lower NPQ values observed.

Assessment of PSI function can corroborate interpretations based on Chl fluorescence. Increases in *in vivo* absorptance at 810 nm are due predominantly to accumulation of oxidized forms

Table 1Comparison of physiological properties for WT and *LHCB7*-deficient arabidopsis (Col background) at three irradiance levels.

Parameter	Irradiance level	Col (WT) N=12	<i>AtLhcb7-1</i> N=11
R_w (s mm ⁻¹)	LL	0.44 ± 0.03	0.53 ± 0.04
	ML	0.48 ± 0.03	0.57 ± 0.06
	HL	0.37 ± 0.02	0.35 ± 0.03
J_c (μmol e ⁻ m ⁻² s ⁻¹)	LL	6.2 ± 0.2	6.4 ± 0.4
	ML	30.4 ± 1.4	23.4 ± 2.6 [*]
	HL	34.0 ± 1.5	27.4 ± 2.6 [*]
NPQ	LL	0.02 ± 0.02	0.11 ± 0.03 [*]
	ML	1.01 ± 0.08	1.32 ± 0.10 [*]
	HL	1.67 ± 0.07	1.82 ± 0.09
qP	LL	0.970 ± 0.003	0.962 ± 0.002 [*]
	ML	0.687 ± 0.017	0.581 ± 0.030 ^{**}
	HL	0.214 ± 0.005	0.183 ± 0.011 ^{**}
F_v/F_m	LL	0.789 ± 0.004	0.756 ± 0.014 [*]
	ML	0.690 ± 0.008	0.642 ± 0.013 [*]
	HL	0.647 ± 0.008	0.613 ± 0.018 [*]
ϕ_2	LL	0.765 ± 0.005	0.728 ± 0.014 ^{**}
	ML	0.474 ± 0.015	0.374 ± 0.021 ^{**}
	HL	0.138 ± 0.004	0.113 ± 0.008 ^{**}
ϕ_1	LL	0.640 ± 0.008	0.667 ± 0.034
	ML	0.486 ± 0.008	0.422 ± 0.015 ^{**}
	HL	0.164 ± 0.003	0.151 ± 0.003 ^{**}
a_2 F_v/F_{md}	LL	0.43 ± 0.02	0.42 ± 0.02
	Dark	0.821 ± 0.004	0.813 ± 0.005

Irradiance levels LL, ML, HL correspond to PADs of 19.7, 200, and 808 μmol quanta m⁻² s⁻¹, respectively, averaged across both lines. Mean PAD at each light level for WT and mutant differed by less than 4%. See text for more information.

* Statistically significant differences due to *AtLHCB7* expression $p < 0.05$.

** Statistically significant differences due to *AtLHCB7* expression $p < 0.01$.

of the PSI primary donor (P700⁺) and the mobile PSI electron donor (plastocyanin (PC⁺)) (Harbinson and Woodward, 1987). Their steady state redox levels in the light reflect a dynamic balance among P700 photo-oxidation, electron donation from PSII, and cyclic electron flow (Harbinson et al., 1990; Laisk et al., 2010). Consequently, a positive albeit frequently nonlinear relationship between ϕ_2 and the photo-oxidizable fraction of the 810-nm signal, ϕ_1 , is observed. The steady state 810-nm signal in actinic light is recorded as W_1 . A 20-ms saturating flash (10000 μmol quanta m⁻² s⁻¹) simultaneously reduces the PQ pool and photo-oxidizes PSI centers possessing acceptor side electron vacancies (Peterson, 2005). Following the flash, PQH₂ reduces the PSI donor side establishing the dark baseline. Thus,

$$\phi_1 = \frac{W_2 - W_1}{A810_{\max}} \quad (6)$$

where $A810_{\max}$ is the full signal obtained by superimposing a 20-ms saturating WL flash on a far red light (FR) background illumination (50 μmol quanta m⁻² s⁻¹, Talts et al., 2007). Table 1 shows that ϕ_1 was lower in *AtLhcb7-1* compared to WT leaves to a relative extent similar to the effect on ϕ_2 .

Confirmation of the *AtLhcb7-1* phenotype

The pattern of enhancement of NPQ and declines in qP , ϕ_2 , and ϕ_1 as irradiance increased suggested reduced assimilatory capacity in *AtLhcb7-1* relative to WT based on responses to manipulation of atmospheric CO₂ level in normal leaves (Peterson, 2005). Since this was unexpected for a PSII antenna protein mutant, we considered the possibility that a cryptic mutation linked to the *AtLHCB7* locus in WiscDsLox506A05 inhibited Calvin cycle function. An isogenic WT control for *AtLhcb7-2* (Fig. 1) was unavailable. Thus, we examined: (1) WT Col plants carrying an *AtLHCB7* antisense transgene and (2) a hemizygous *AtLHCB7* knockout line obtained

by crossing *AtLhcb7-1* and *AtLhcb7-2*. The effect of a hidden mutation in *AtLhcb7-1* would be masked by the normal allele donated by *AtLhcb7-2* in the hemizygote (*AtLhcb7-1/2*). Effects of light level on several parameters for transgenic and *AtLhcb7-1/2* plants as well as WT and *AtLhcb7-1* are shown in Table 2. To enhance sensitivity, each entry is a ratio of measurements at two light levels. Parameters other than NPQ are normalized relative to LL (minimal downregulation of quantum yield). Since NPQ is maximal in HL (Fig. 2), measurements were normalized to HL. Overall, the pattern of change observed for WT versus *AtLhcb7-1* was also observed for WT versus hemizygous mutant and transgenic plants ruling out interference by a second mutation. Exceptions were F_v/F_m for the antisense plants at both irradiance ratios and *AtLhcb7-1* and *AtLhcb7-1/2* for the HL/LL comparisons. Since NPQ suppresses both F_m and F_o (Fig. 3), F_v/F_m is less sensitive to changes in thermal dissipation.

Loss of *AtLHCB7* expression enhances PQH₂ accumulation

Oxidation of PQH₂ is a control point in the PSII-PSI electron transport sequence H₂O → Q_A → Q_B → PQ → Cyt f → PC → P700 (Foyer et al., 1990). Transient changes in the *in vivo* 810-nm signal under a FR background following cessation of actinic WL were used to quantify electron donor pools upstream from PSI, primarily PQH₂ (Asada et al., 1992, 1993). Fig. 4 shows that the drop in excitation of PSI caused by interruption of actinic WL (panels B, C, and inset) resulted in rapid reduction of the PSI donor side followed by a slower FR-dependent re-oxidation as equivalents from PQH₂ were transferred via P700 to the acceptor side of PSI. Integration of the signal change time course (complementary area, CA) constitutes a relative approximation of the size of the electron reservoir upstream of PSI under the steady state WL+FR. Leaves of WT showed a >3-fold increase in CA in HL (Fig. 4C) compared to ML (Fig. 4B) consistent with higher feedback downregulation of

Table 2Normalized responses to irradiance relative to WT for knockout strains (*AtLhcb7-1*, *AtLhcb7-1/2*) and plants possessing an antisense construct against *AtLHC7*.

Parameter	Irradiance ratio	WT (Col) N=12	<i>AtLhcb7-1</i> N=11	Antisense <i>AtLhcb7</i> N=15	F1 cross <i>AtLhcb7-1/2</i> N=9
ϕ_s	ML/LL	0.477 ± 0.028	0.377 ± 0.034*	0.379 ± 0.015**	0.350 ± 0.010**
	HL/LL	0.132 ± 0.007	0.109 ± 0.008*	0.104 ± 0.005**	0.098 ± 0.004**
<i>qP</i>	ML/LL	0.708 ± 0.018	0.604 ± 0.030**	0.648 ± 0.019*	0.563 ± 0.019**
	HL/LL	0.220 ± 0.005	0.190 ± 0.011**	0.189 ± 0.011*	0.168 ± 0.013**
ϕ_2	ML/LL	0.620 ± 0.018	0.514 ± 0.028**	0.565 ± 0.020*	0.468 ± 0.023**
	HL/LL	0.181 ± 0.005	0.154 ± 0.008**	0.157 ± 0.009*	0.135 ± 0.011**
ϕ_1	ML/LL	0.760 ± 0.015	0.644 ± 0.030**	0.675 ± 0.025**	0.594 ± 0.018**
	HL/LL	0.257 ± 0.007	0.231 ± 0.009*	0.228 ± 0.010*	0.225 ± 0.009**
F_v/F_m	ML/LL	0.875 ± 0.006	0.849 ± 0.007**	0.870 ± 0.009	0.829 ± 0.018**
	HL/LL	0.820 ± 0.007	0.809 ± 0.012	0.832 ± 0.007	0.802 ± 0.018
NPQ	LL/HL	0.006 ± 0.013	0.056 ± 0.016*	0.049 ± 0.009**	0.044 ± 0.018*
	ML/HL	0.601 ± 0.036	0.722 ± 0.039*	0.689 ± 0.026*	0.717 ± 0.037*

The first five parameters show the ratio of the value obtained in ML or HL to that obtained in LL. NPQ values are normalized to HL. Means for knockout and antisense plants are statistically compared to WT using a T-test. Asterisks are defined in Table 1. See text and Table 1 for additional information.

light utilization at the saturating HL level. No reduction transient was detected in LL (Fig. 4A) confirming a lack of PQH₂ accumulation when PSII turnover limits the linear electron transport rate. Most important, average CA values for *AtLhcb7-1* were 66% and 24% larger than WT in ML and HL, respectively, consistent with enhanced PQH₂ accumulation in the mutant. We note also a detectably slower rise in the 810-nm signal for the mutant consistent with restricted oxidation of NADPH downstream from PSI (Fig. 5).

The transients of Fig. 4 are subject to minor distortion for two reasons. First, due to differences in the extinction coefficients for PC⁺ and P700⁺ and the midpoint redox potentials of these carriers the incremental change in the 810-nm signal per incremental change in reduction of the PSI primary donors is not constant (Oja et al., 2003). This ratio increases with the magnitude of the 810-nm signal. Secondly, return of electrons from the PSI acceptor side to PC⁺ and P700⁺ via a cyclic pathway would falsely inflate the CA values (Asada et al., 1993). Indeed, FR-driven PSI cyclic electron flow is favored with increasing oxidation of PC and P700 (Talts et al., 2007; Laisk et al., 2010). Since, on average, the 810-nm signal is slightly (6–7%) higher for WT in ML and HL compared to mutant leaves over the 3-s interval used for assessment of CA we conclude that overestimation of CA is greater for WT. Consideration of these effects would magnify the increase in CA for *AtLhcb7-1* relative to WT. Lastly, the steady state signal attained after 2 s of FR (Fig. 4A) was essentially identical for WT (77.0% ± 0.5) and mutant (77.7% ± 0.4) suggesting no difference between these lines in FR-driven cyclic electron flow.

No effect of *AtLHC7* deficiency on V de-epoxidation

The pH-dependent conversion of V to Z by V de-epoxidase in the thylakoid lumen is associated with light-dependent formation of NPQ and the protonmotive force for ATP formation (Demmig-Adams, 1990; Hager and Holcher, 1994; Avenson et al., 2004). Fig. 5 indicates no enhancement of V de-epoxidation in *AtLhcb7-1* compared to WT. Despite incomplete reversal of A and Z accumulation in the dark, a 3-fold increase in de-epoxidation was observed saturating at a PFD of 700 μmol quanta m⁻² s⁻¹. Two-way ANOVA confirmed that the effect of genotype was not statistically significant ($p = 0.39$).

Discussion

Although challenging to characterize, weak phenotypes such as *AtLHC7*-deficiency offer a rare advantage for probing the biochemical subtleties of photosynthetic regulation. Specifically, our assessment of *AtLHC7* function is unlikely to be confounded by gross effects on PSII integrity. We observed no effect on PSII

absorption cross section (a_2), F_v/F_{md} , and absorptance of WL. The apparent lack of effect of *AtLHC7*-deficiency on pigment levels or compensatory change in *AtLHC1-6* content could be related to the limited expression of *AtLHC7*. The “rarely expressed” genes *AtLHC6*, *AtLHC7*, and *AtLHC8* (Klimmek et al., 2006) were found to be well expressed in a subset of cells in various tissue loci (Sawchuk et al., 2008). Expression of *AtLHC7* occurred exclusively in mesophyll cells near the adaxial surface of the leaf. The normally higher excitation levels in these cells led Sawchuk et al. to suggest that *AtLHC7* has a photoprotective role. On the contrary, our results indicate that maximal NPQ is unaffected by *AtLHC7* content and NPQ induction is shifted to a higher irradiance range in WT leaves. By contrast, V de-epoxidase, psbS, or lycopene ε-cyclase level does affect maximal NPQ capacity (Müller et al., 2001). Loss of *AtLHC7* expression is associated with depressed rates of electron transport (J_c), higher PQH₂ levels (CA), and lower open PSII trap density (*qP*) and PSI/PSII quantum yields (ϕ_1 , ϕ_2) characteristic of response to a downstream limitation in assimilatory capacity (Genty et al., 1989; Harbinson et al., 1990; Peterson, 2005). This altered regulatory pattern is maintained in an *AtLHC7* antisense line and in the *AtLhcb7-1/2* hemizygote (Table 2) ruling out interference by a cryptic, second mutation affecting carbon fixation.

A conceptual organizing principle of photosynthetic regulation is that Rubisco activity is coordinated with PSII, PSI, and cytochrome (Cyt) b_{6f} function; broadly referred to as “photosynthetic control” (Genty et al., 1989; Foyer et al., 1990; Eichelmann et al., 2009). Manifestations of this control are NPQ; accumulation of Q_A⁻, PQH₂, PC⁺, and P700⁺; closure of PSI centers by acceptor side reduction; and resistance to electron transfer from PQH₂ to Cyt f. Accumulation of H⁺ ions in the thylakoid lumen orchestrates these responses. The dominant *qE* phase of NPQ is considered to follow protonation of sites in the PSII antenna inducing a conformational change aided by A and Z accumulation (Krause, 1973; Hager and Holcher, 1994; Horton et al., 1996; Gilmore, 1997; Avenson et al., 2004; Ruban et al., 2001, 2007). Co-transport of electrons and H⁺ during PQH₂ oxidation is opposed by luminal H⁺ leading to higher reduction of Q_A (Sigel, 1974; Harbinson and Hedley, 1989). The luminal pH is maintained at a moderate 5.8–6.5, permitting ATP synthesis and regulation while avoiding H⁺-induced damage (Kramer et al., 1999; Zaks et al., 2012). Thus, effects of loss of *AtLHC7* expression are consistent with imposition of photosynthetic control mediated by luminal pH. An intriguing possibility is that the antenna component *AtLHC7* could be the postulated messenger linking photochemical yield and Rubisco Activase function which controls Rubisco active site turnover (Eichelmann et al., 2009).

The significant shifts in light-dependent induction of NPQ (Fig. 2) and *qP* (Fig. 3) contrast with phenotypes selected for altered thermal dissipation capacity. Arabidopsis mutants deficient in NPQ such

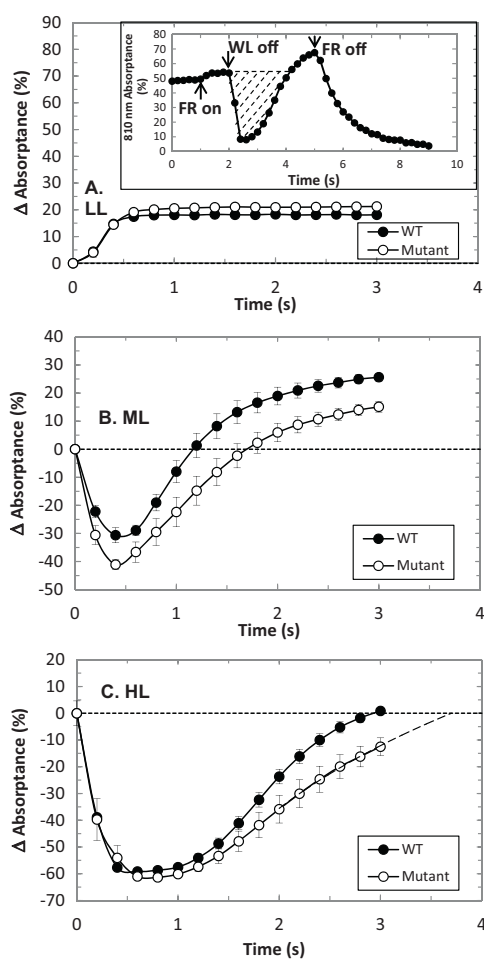


Fig. 4. Assessment of PQH_2 pool size in WT and *AtLhcb7-1*. The inset shows a recording (0.2-s intervals) of *in vivo* absorptance at 810 nm expressed as percent of maximum ($A_{810\text{nm}}$) where zero corresponds to full reduction and 100 represents full oxidation of PC and P700 for a mutant leaf pre-illuminated with ML. After attainment of the steady state signal level in WL, PSI-specific FR ($50 \mu\text{mol quanta m}^{-2} \text{s}^{-1}$) was superimposed causing a slight increase in signal which stabilized within 0.4 s. Sudden interruption of the WL caused a transient, nearly complete reduction of the primary electron donor pool of PSI followed by re-oxidation in FR. After 3 s the FR was turned off and the signal was recorded for an additional 4 s in darkness. The region (diagonal dashed lines) bounded by the recorded signal and the steady state response in FR+WL (horizontal dashed baselines in inset and main panels) was calculated as $\sum(\Delta\text{Absorptance} \times 0.2 \text{ s})$ and defined as the CA. Main panels A–C show averaged $\Delta\text{Absorptance}$ profiles during the FR-only phase for the experiments of Table 1 wherein pre-illumination was supplied by LL, ML, and HL levels of WL, respectively. Ordinate zero levels correspond to the mean signal level just prior to removal of WL. Mean ($\pm\text{SE}$) CA values (% s) in ML for WT and mutant were 25.1 ± 4.3 and 41.6 ± 5.2 , respectively. Corresponding means in HL were 101.8 ± 2.6 and 126.5 ± 5.0 . The effect of genotype was significant ($p \leq 0.01$) at both light levels based on a *T*-test. The CA at LL was undetectable (panel A). In some instances the 3-s FR illumination was not sufficient to restore the signal to the FR+WL level (panel C). In these cases, the tail was extended by fitting to a logarithmic function.

as *Npq4* (Li et al., 2000; Peterson, 2005) and *que* (Kalituhu et al., 2006) exhibited higher reduction of Q_A (lower qP) compared to WT under identical conditions of measurement. Conversely, overexpression of *AtPsbS* resulted in enhancement of both *NPQ* and qP (Li et al., 2002). This positive relationship between *NPQ* and qP contrasts with the properties of *AtLhcb7-1*. In the mutant, *NPQ* equaled or exceeded that of WT yet qP was consistently lower. Despite the lack of conformity of *AtLhcb7-1* to other variants possessing a modified PSII, the homology of LHC7 to PSII antenna proteins (Klimmek et al., 2006) prompts some consideration of a PSII centered interpretation of the *AtLhcb7-1* phenotype perhaps in which increased *NPQ* is linked to slower Q_A^- oxidation via a conformational change.

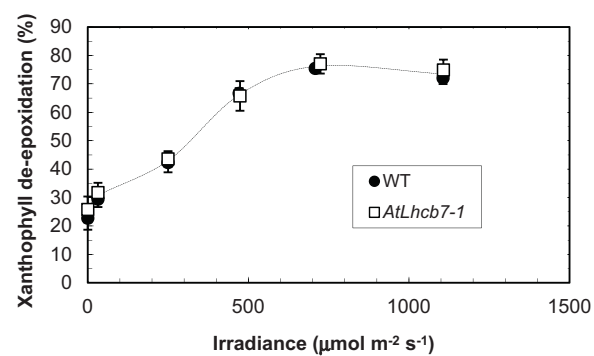


Fig. 5. Light dependence of V de-epoxidation in WT and *AtLhcb7-1*. Excised leaves were floated on distilled H_2O in Petri plates and pre-illuminated for 2 h at a PFD of $250 \mu\text{mol quanta m}^{-2} \text{s}^{-1}$ and 23°C . The leaves were then darkened for 30 min prior to a 30-min exposure to WL at the indicated PFD levels. Pigments were extracted with acetone and separated and quantified by HPLC (see Materials and methods). Per cent V de-epoxidation was calculated as $100 \times (Z + 0.5 \times A)/(V + A + Z)$. Separate time course experiments showed that the extent of V de-epoxidation leveled within 30 min.

Fortunately, the two distinct interpretations of the *AtLHC7*-deficient phenotype introduced here can be resolved. From the perspective of control of interphotosystem electron transport, upstream limitation (PSII function) should lower, while downstream limitation (Rubisco turnover) should raise, the PQH_2 level. Thus, it is sufficient to ascertain whether PQH_2 is less or more abundant in the mutant compared to WT under the same conditions. Analysis of changes in the 810-nm absorptance signal from PSI is beset by contributions from multiple chromophores and co-existence of linear and cyclic electron flows (Oja et al., 2003; Talts et al., 2007; Laisk et al., 2010). These factors were considered in our analyses of CA (Fig. 4). We conclude that the PQH_2 pool is larger for the mutant when photons are present in excess confirming the downstream limitation alternative for electron transport rate.

Although higher levels of PQH_2 for *AtLhcb7-1* are consistent with a lower luminal pH compared to WT this did not result in higher Z levels in the mutant as would be expected based on simple pH control of V de-epoxidase. Lower V de-epoxidation correlated with impaired transthylakoid ΔpH formation in an *AtLHC6* knockout (Bianchi et al., 2008). On the other hand, several studies suggest that this pH-control model is insufficient. Differential effects on the relative activities of V de-epoxidase and Z epoxidase can result in shifts in the extent of accumulation of Z in response to transthylakoid ΔpH (Zhang et al., 2011). Using reflectance measurements to monitor Z levels *in vivo*, Peguero-Pina et al. (2013) described a complex relationship between NPQ and Z in *Quercus coccifera*. Three Z pools were identified and postulated to have different roles in photoprotection. In this study, the effect of a lower luminal pH in *AtLhcb7-1* may be offset by lower levels of ascorbate, a substrate for the V de-epoxidase reaction (Hager, 1969). Lower rates of linear electron transport in the mutant could lead to competition for NADPH between 3-phosphoglyceric acid reduction and conversion of monodehydroascorbate to ascorbate (Müller-Moulé et al., 2002).

Acknowledgements

This work was supported by Hatch funds from the US Department of Agriculture. We thank Carol Clark and Regan Huntley for skillful technical assistance and Neil McHale for helpful conversations.

References

- Alboresi A, Caffarri S, Nogue F, Bassi R, Morosinotto T. *In silico* and biochemical analysis of *Physcomitrella patens* photosynthetic antenna: identification of subunits which evolved upon land adaptation. *PLoS ONE* 2008;3(4):e2033.

- Allen JF, de Paula WBM, Puthiyaveetil S, Nield J. A structural phylogenetic map for chloroplast photosynthesis. *Trends Plant Sci* 2011;16:645–55.
- Alonso JM, Stepanova AN, Leisse TJ, Kim CJ, Chen H, Shinn P, et al. Genome-wide insertional mutagenesis of *Arabidopsis thaliana*. *Science* 2003;301:653–7.
- Andersson J, Walters RG, Horton P, Jansson S. Antisense inhibition of the photosynthetic antenna proteins CP29 and CP26: implications for the mechanism of protective energy dissipation. *Plant Cell* 2001;13:1193–204.
- Andersson J, Wentworth M, Walters RG, Howard CA, Ruban AV, Horton P, et al. Absence of the LhcB1 and LhcB2 proteins of the light-harvesting complex of photosystem II-effects on photosynthesis, grana stacking and fitness. *Plant J* 2003;35:350–61.
- Asada K, Heber U, Schreiber U. Pool size of electrons that can be donated to P700⁺, as determined in intact leaves: donation to P700⁺ from stromal components via the intersystem chain. *Plant Cell Physiol* 1992;33:927–32.
- Asada K, Heber U, Schreiber U. Electron flow to the intersystem chain from stromal components and cyclic electron flow in maize chloroplasts, as detected in intact leaves by monitoring redox change of P700 and chlorophyll fluorescence. *Plant Cell Physiol* 1993;34:39–50.
- Avenson TJ, Cruz JA, Kramer DM. Modulation of energy-dependent quenching of excitons in antennae of higher plants. *Proc Natl Acad Sci U S A* 2004;101:5530–5.
- Bianchi SD, Dall'Osto L, Tognon G, Morosinotto T, Bassi R. Minor antenna proteins CP24 and CP26 affect interactions between photosystem II subunits and the electron transport rate in grana membranes of *Arabidopsis*. *Plant Cell* 2008;20:1012–28.
- Clough SJ, Bent AF. Floral dip: a simplified method for *Agrobacterium*-mediated transformation of *Arabidopsis thaliana*. *Plant J* 1998;16:735–43.
- Dau H. Molecular mechanism and quantitative models of variable Photosystem II fluorescence. *Photochem Photobiol* 1994;60:1–23.
- Dekker JP, Boekema EJ. Supramolecular organization of thylakoid membrane proteins in green plants. *Biochim Biophys Acta* 2005;1706:12–39.
- DellaPorta SL. Plant DNA miniprep and microprep: Version 2.1–2.3. In: Freeling M, Walbot V, editors. *The maize handbook*. New York: Springer-Verlag; 1993. p. 522–5.
- Demmig-Adams B. Carotenoids and photoprotection: a role for the xanthophyll zeaxanthin. *Biochim Biophys Acta* 1990;1020:1–24.
- Eichelmann H, Talts E, Oja V, Padu E, Laisk A. Rubisco in *planta* k_{cat} is regulated in balance with photosynthetic electron transport. *J Exp Bot* 2009;60: 4077–88.
- Foyer C, Furbank R, Harbinson J, Horton P. The mechanisms contributing to photosynthetic control of electron transport by carbon assimilation in leaves. *Photosynth Res* 1990;25:83–100.
- Ganeteg U, Kühlheim C, Andersson J, Jansson S. Is each light-harvesting complex protein important for plant fitness. *Plant Physiol* 2004;134:502–9.
- Genty B, Briantais J-M, Baker NR. The relationship between the quantum yield of photosynthetic electron transport and quenching of chlorophyll fluorescence. *Biochim Biophys Acta* 1989;990:87–92.
- Gilmore AM. Mechanistic aspects of xanthophyll cycle-dependent photoprotection in higher plant chloroplasts and leaves. *Physiol Plant* 1997;99:197–209.
- Green BR, Durnford DG. The chlorophyll-carotenoid proteins of oxygenic photosynthesis. *Annu Rev Plant Physiol Plant Mol Biol* 1996;47:685–714.
- Hager A. Lichtbedingte pH-Erniedrigung in einem Chloroplasten-Kompartiment als Ursache der enzymatischen Violaxanthin-Zeaxanthin-Umwandlung: Beziehung zur Photophosphorylierung. *Planta* 1969;89:224–43.
- Hager A, Holocher K. Localization of the xanthophyll-cycle enzyme violaxanthin de-epoxidase within the thylakoid lumen and abolition of its mobility by a (light-dependent) pH decrease. *Planta* 1994;192:581–9.
- Harbinson J, Hedley CL. The kinetics of P700⁺ reduction in leaves: a novel in situ probe of thylakoid functioning. *Plant Cell Environ* 1989;12:357–69.
- Harbinson J, Woodward FI. The use of light-induced absorbance changes at 820 nm to monitor the oxidation state of P-700 in leaves. *Plant Cell Environ* 1987;10:131–40.
- Harbinson J, Genty B, Baker NR. The relationship between CO₂ assimilation and electron transport in leaves. *Photosynth Res* 1990;25:213–24.
- Horton P, Ruban AV, Walters RG. Regulation of light harvesting in green plants. *Annu Rev Plant Physiol Plant Mol Biol* 1996;47:655–84.
- Jansson S. A guide to the Lhc genes and their relatives in *Arabidopsis*. *Trends Plant Sci* 1999;4:236–40.
- Kaltiuhu L, Graßes T, Graf M, Rech J, Jahns P. Characterization of a nonphotochemical quenching-deficient *Arabidopsis* mutant possessing an intact PsbS protein, xanthophyll cycle and lumen acidification. *Planta* 2006;223:532–41.
- Klimmek F, Sjödin A, Noutsos C, Leister D, Jansson S. Abundantly and rarely expressed Lhc protein genes exhibit distinct regulation patterns in plants. *Plant Physiol* 2006;140:793–804.
- Kovács L, Damkjær J, Kerecche S, Illoia C, Ruban AV, Boekema EJ, et al. Lack of the light-harvesting complex CP24 affects the structure and function of the grana membranes of higher plant chloroplasts. *Plant Cell* 2006;18:3106–20.
- Kramer DM, Sacksteder CA, Cruz JA. How acidic is the lumen? *Photosynth Res* 1999;60:151–63.
- Krause GH. The high-energy state of the thylakoid system as indicated by chlorophyll fluorescence and chloroplast shrinkage. *Biochim Biophys Acta* 1973;292:715–28.
- Laisk A, Loreto F. Determining photosynthetic parameters from leaf CO₂ exchange and chlorophyll fluorescence: Rubisco specificity factor, dark respiration in the light, excitation distribution between photosystems, alternative electron transport and mesophyll diffusion resistance. *Plant Physiol* 1996;110:903–12.
- Laisk A, Oja V, Rasulov B, Rämäma H, Eichelmann H, Kasparova I, et al. A computer-operated routine of gas exchange and optical measurements to diagnose photosynthetic apparatus in leaves. *Plant Cell Environ* 2002;25:923–43.
- Laisk A, Talts E, Oja V, Eichelmann H, Peterson RB. Fast cyclic electron transport around photosystem I in leaves under far-red light: a proton-uncoupled pathway? *Photosynth Res* 2010;103:79–95.
- Li X-P, Björkman O, Shih C, Grossman AR, Rosenquist M, Jansson S, et al. A pigment-binding protein essential for regulation of photosynthetic light harvesting. *Nature* 2000;403:391–5.
- Li X-P, Müller-Moulé P, Gilmore AM, Niyogi KK. PsbS-dependent enhancement of feedback de-excitation protects photosystem II from photoinhibition. *Proc Natl Acad Sci U S A* 2002;99:15222–7.
- Müller P, Li X-P, Niyogi KK. Non-photochemical quenching. A response to excess light energy. *Plant Physiol* 2001;125:1558–66.
- Müller-Moulé P, Conklin PL, Niyogi KK. Ascorbate deficiency can limit violaxanthin de-epoxidase activity *in vivo*. *Plant Physiol* 2002;128:970–7.
- Oja V, Eichelmann H, Peterson RB, Rasulov B, Laisk A. Deciphering the 820 nm signal: redox state of donor side and quantum yield of photosystem I in leaves. *Photosynth Res* 2003;78:1–15.
- O'Malley RC, Ecker JR. Linking genotype to phenotype using the *Arabidopsis* unimutant collection. *Plant J* 2010;61:928–40.
- Peguero-Pina JJ, Gil-Peláez E, Morales F. Three pools of zeaxanthin in *Quercus coccifera* leaves during light transitions with different roles in rapidly reversible photoprotective energy dissipation and photoprotection. *J Exp Bot* 2013;64:1649–61.
- Peterson RB. PsbS genotype in relation to coordinated function of PS II and PS I in *Arabidopsis* leaves. *Photosynth Res* 2005;85:205–19.
- Peterson RB, Havir EA. A nonphotochemical-quenching-deficient mutant of *Arabidopsis thaliana* possessing normal pigment composition and xanthophyll-cycle activity. *Planta* 2000;210:205–14.
- Peterson RB, Havir EA. Photosynthetic properties of an *Arabidopsis thaliana* mutant possessing a defective psbS gene. *Planta* 2001;214:142–52.
- Peterson RB, Havir EA. The multiphasic nature of nonphotochemical quenching: implications for assessment of photosynthetic electron transport based on chlorophyll fluorescence. *Photosynth Res* 2004;82:95–107.
- Peterson RB, Oja V, Laisk A. Chlorophyll fluorescence at 680 and 730 nm and leaf photosynthesis. *Photosynth Res* 2001;70:185–96.
- Ruban AV, Wentworth M, Horton P. Kinetic analysis of nonphotochemical quenching of chlorophyll fluorescence. 1. Isolated chloroplasts. *Biochemistry* 2001;40:9896–901.
- Ruban AV, Berera R, Illoia C, van Stokkum IHM, Kennis JTM, Pascal AA, et al. Identification of a mechanism of photoprotective energy dissipation in higher plants. *Nature* 2007;450:575–9.
- Sawchuk MG, Donner TJ, Head P, Scarpella E. Unique and overlapping expression patterns among members of photosynthesis-associated nuclear gene families in *Arabidopsis*. *Plant Physiol* 2008;148:1908–24.
- Sigell U. The control of electron transport by two pH-sensitive sites. In: Avron M, editor. *Proceedings 3rd Intern Congr Photosynth. Amsterdam*: Elsevier; 1974. p. 645–54.
- Sundaresan V, Springer P, Volpe T, Haward S, Jones J, Dean C, et al. Patterns of gene action in plant development revealed by enhancer trap and gene trap transposable elements. *Genes Dev* 1995;9:1797–810.
- Talts E, Oja V, Rämäma H, Rasulov B, Anijalg A, Laisk A. Dark inactivation of ferredoxin-NADP reductase and cyclic electron flow under far-red light in sunflower leaves. *Photosynth Res* 2007;94:109–20.
- Timmermans MCP, Maliga P, Vieira J, Messing J. The pFF plasmids: cassettes utilizing CaMV sequences for expression of foreign genes in plants. *J Biotechnol* 1990;14:333–44.
- Woody ST, Austin-Phillips S, Amasino RM, Krysan PJ. The *WiscDsLox* T-DNA collection: an *Arabidopsis* community resource generated by using an improved high-throughput T-DNA sequencing pipeline. *J Plant Res* 2007;120:157–65.
- Zaks J, Amarnath K, Kramer DM, Niyogi KK, Fleming GR. A kinetic model of rapidly reversible nonphotochemical quenching. *Proc Natl Acad Sci U S A* 2012;109:15757–62.
- Zhang R, Kramer DM, Cruz JA, Struck KR, Sharkey TD. The effects of moderately high temperature on zeaxanthin accumulation and decay. *Photosynth Res* 2011;108:171–81.